JOURNAL OF MATERIALS SCIENCE: MATERIALS IN MEDICINE 4 (1993) 471 – 480

Evaluation of an elastomer for biomedical use in load-bearing applications

Part I *In vitro fatigue testing*

J. A. HELSEN, S. V. JAECQUES, J. VAN HUMBEECK
Department of Metallurgy and Materials Engineering, KU Leuven, De Croylaan 2, B-3001 Leuven, Belgium

J.-P. SIMON
Department of Orthopaedic Surgery, Orthopaedic Hospital, KU Leuven, B-3212 Pellenberg, Belgium

The fatigue behaviour of a medical-grade thermoplastic polyolefin (TPO) was investigated with the objective of using TPOs for endoprosthetical aims in dental and orthopaedic applications. For this purpose, a TPO was subjected to the combined action of shear and compression fatigue while in contact with Hanks' solution. Cyclic loading between 150 and 1500 kPa shear stress and a number of cycles up to 9×10^6 was applied. The potential fatigue damage was assessed by in-fatigue-recording of the mechanical hysteresis curves and, after fatigue, by swelling tests in acetic acid solutions, dynamic mechanical thermal analysis, Fourier transform infrared spectroscopy, X-ray diffraction and scanning electron microscopy. The combined and critical application of these techniques allowed us to conclude that this material exhibits a very satisfactory fatigue behaviour under the loads investigated, making this material potentially useful for endoprostheses. Moreover, biomedical prescreening tests (according to USP Class VI) were all negative, stimulating continued research on this type of material.

1. Introduction

A new generic class of rubbers, called "thermoplastic elastomers" (TPEs) was introduced as an innovative product on the rubber market in the early seventies. The production and application of these elastomers has steadily grown since their introduction, a growth increasing to about 6% annually during the last decade. The production covers, worldwide, approximately 5% of the global rubber market and the growth was performed at the expense of the classical thermoset rubbers [1]. Application in the biomedical field in general, however, did not show the same growth perspective. For permanent endodevices, thermoplastic polyurethanes are almost the only TPEs used.

TPEs exhibit behaviour similar to the classic natural and synthetic rubbers but can be processed like conventional plastics by injection moulding or extrusion. This aspect is industrially important for applications where oddly shaped objects have to be produced. A disadvantage of TPEs as compared to thermoset rubbers is their higher sensitivity to creep.

The thermoplastic polyolefins (TPOs) form a subclass of TPEs, consisting of blends of semicrystalline thermoplasts and amorphous elastomers. They seemed to exhibit a number of attractive properties potentially suitable for load-bearing medical applications. The results presented in this first paper were obtained not on a commercially available product but on a laboratory-made version of the same composition. The components of the TPO were all FDA-regulated compounds meeting USP Class VI [2] requirements and processing was performed in specially purged equipment with no residue from previous batches. All products referred to hereafter as "medical grades" meet these specifications. The TPO consists of a blend of polypropene and EPDM, the first being responsible for the thermoplastic behaviour and the second for its elastomeric properties. EPDM is a terpolymer, i.e. copolymerized ethene and propene and as third monomer a non-conjugated diene. The main properties of TPOs are [3]: (a) temperature range of useful mechanical properties between -40 and $+150\,^{\circ}C$; (b) low compression and tension set; (c) low swelling in contact with aqueous solutions; (d) high tear strength; (e) good abrasion resistance; (f) excellent fatigue resistance; (g) hardness range from 55 Shore A to 40 Shore D (by varying the polypropylene/EPDM ratio of the blend).

Before starting extensive mechanical and biomedical testing, a preliminary biocompatibility study was undertaken according to the procedures required by the US Pharmacopeia for Class VI plastics.

The materials used are outlined in Table I together with the codes by which they will be referred to throughout the text.

Acute systemic toxicity was tested with extracts of TPO in sodium chloride, a mixture of ethanol and sodium chloride, polyethylene glycol and cottonseed

0957–4530

TABLE I Codes for the materials tested

Code	Description
PP	Polypropene[a]
EPDM	EPDM – rubber[a]
2-80	TPO, hardness 80 Shore A
2-87	*Idem*, 87 Shore A
3-82	TPO, medical grade, hardness 82 Shore A

[a]Representative of the raw materials used in the manufacturing of the TPO. Manufacturing was done by blending of PP and EPDM; the latter was simultaneously vulcanized. The blend was then injection moulded into plaques of 2 mm thickness.

oil. These extracts were then injected in young and healthy albino mice; five animals received the TPO extract and the remaining five the pure solution as control. No significant difference was found between the TPO extract and the pure control solutions. Intracutaneous toxicity was tested using the same extracts as for the systemic toxicity test. Two New Zealand white rabbits were used for each extract. There was no significant difference between extract and control. Cytotoxicity was tested on L-929 fibroblastic mice cells as described in the ASTM F813 [4] norm. The test was performed with TPO 2-87, USP negative-control plastic as negative control and M-8001 as positive control. The TPO did not appear to be toxic to the mice cells. The haemolysis test showed 0% haemolysis on rabbit blood. In the muscle implantation test, upon visual inspection no significant macroscopic difference was found between the TPO and negative control plastic. Only upon microscopic investigation was the TPO found to be a slight irritant compared to the negative control.

Because all these tests definitely suggested acceptable biocompatibility, it was decided to proceed to an extensive testing of the fatigue performance of the TPO and in particular of the medical grade, 3-82. As the first tests were positive here too, a complete evaluation programme was set up to investigate the suitability of this material for hard-tissue replacement in orthopaedic and dental applications. The loads were chosen in the orthopaedic range. To reduce the number of parameters involved, fatigue testing was restricted to 2-80 and 3-82. These grades have a hardness midway in the suitable range (70–90 Shore A) for this kind of application. Potential fatigue damage under cyclic loading was assessed by a wide variety of experimental techniques: evolution of stress–strain behaviour during fatigue, dynamic mechanical thermal analysis (DMTA), Fourier transform infrared spectroscopy (FTIR), X-ray diffraction (XRD), swelling in different solvents, SEM and optical microscopy. The main results are the subject of this paper. Parallel to the mechanical testing and encouraged by the good results, *in vitro* (cell cultures) and *in vivo* experiments (implantation in test animals) were also started.

These experiments, as well as the previously mentioned "US Pharmacopeia Class VI" tests will be reported and fully discussed in a second paper. Finally, a third paper will report the evaluation of applications.

For all these experiments, the intermediate results are encouraging. As already mentioned, no biomedical applications of the present material have been reported. Recently, however, Mast and Huysmans presented a preliminary report on the growth of fibroblasts on the surface of EPDM rubbers as a poster on the IVth World Biomaterials Congress in Berlin (24–28 April 1992) [5]. These authors investigated the growth curves of human fibroblasts on EPDM rubbers as a substrate. The growth curves did not differ significantly from control curves. Long-term extrapolation of these results is not permitted yet, but these results do certainly corroborate the perspectives opened by our experiments and are stimulating continued research on this topic.

2. Experimental procedure

2.1. Fatigue

The experimental apparatus is shown in Fig. 1. Samples of $2 \times 20 \times 25$ mm^3 were glued to the stationary part of the sample holder (i.e. the stamp) with cyanoacrylate adhesive (Locktite 406) after being prepared with a primer (Locktite 457). The machine used to apply cyclic load was a Schenck computer-monitored hydraulic compression fatigue machine capable of a maximum load of 7 kN. Forces were measured with a Schenck force transducer model PM 10 Rn and displacements with a Schenck displacement transducer. The stamp was fixed to the force transducer and the load was applied to the anvil by a hydraulic cylinder. The recipient containing the Hanks' solution was sealed to the anvil and moved up and down with it.

The applied fatigue conditions are summarized in Table II. In all experiments, the sinusoidal fatigue mode was used and force was varied between 150 and

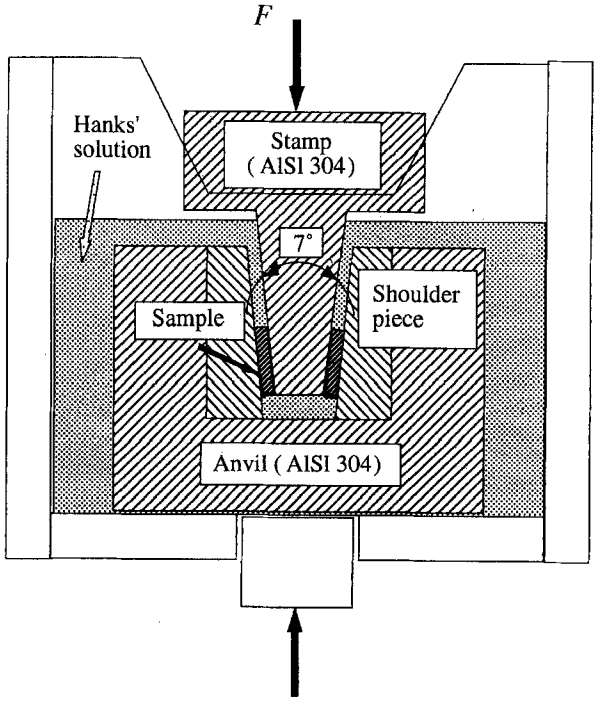

Figure 1 Cell for fatigue testing in air or in contact with liquids. Load angle = 3.5°.

TABLE II Data of fatigue tests

ID code	Grade	Environment	Number of cycles (10^6)	Fatigue mode[a]
1.1	2-80	Hanks'	6.7	F
1.2	2-80	Hanks'	6.25	F
1.3	2-80	Hanks'	5.7	F
1.4	2-80	Hanks'	5.9	F
2.1	3-82	Air	1.7	D
2.2	3-82	Air	7.0	D
2.3	3-82	Hanks'	6.5	D
2.4	3-82	Hanks'	5.4	D
2.5	3-82	Air	1.7	F
2.6	3-82	Air	4.9	F
2.7	3-82	Hanks'	5.4	D
2.8	3-82	Hanks'	3.6	F
2.9	3-82	Hanks'	1.84	D
2.10	3-82	Hanks'	0.41	F
2.11	3-82	Air	1.9	F
2.12	2-80	Air	3.3	F
2.13	3-82	Hanks'	12	D
2.14	3-82	Air	0.25	F

[a]F = force, D = displacement.

1500 N. Owing to the geometry, these forces cause mainly shear stress with compressive stress only $\approx 8\%$ of shear stress.

For additional fatigue testing, a constant displacement device was constructed in which the force was applied by a variable speed d.c. motor via a crank and crankshaft mechanism. Displacement was fixed at 0.53 mm. Force was monitored with a Schenck PM 10 Rn force transducer and the sample mounting height was adjusted at regular intervals to maintain the force amplitude at approximately 1500 N. This results in a shear stress of 1497 kPa and a normal stress of 92 kPa. The number of cycles was registered by an electromechanical counter.

During the fatigue test, the following data were recorded from the Schenck machine by a Data Harvester: number of cycles, instantaneous force and displacement. Computer handling of these data allows hysteresis curves to be constructed and to perform other scalar operations. After fatigue testing, the damage was assessed by comparing a set of properties of fatigued and control samples of the same production batch.

2.2. Swelling

Liquid absorption (swelling) was determined both as relative mass change (% δ_m), expressed by

$$\% \delta_m = \frac{m(t) - m(0)}{m(0)} \times 100 \quad (1)$$

and as relative thickness change (% δ_l), expressed by

$$\% \delta_l = \frac{l(t) - l(0)}{l(0)} \times 100 \quad (2)$$

where (t) and (0) are referred, respectively, to mass or thickness at time $t = 0$ and $t = t$. The liquids used were tetrabutylammoniumhydroxide (TBA), acetic acid 3%(vol/vol) (HAc), toluene, H_2O, H_2O + 2% (vol/vol) zwitterionic detergent with molecular weights of 279.4 (Zwittergent 8), 335.4 (Zwittergent 12) and 391.6 (Zwittergent 16; Zwittergent™, Calbiochem-Behring Corp., CA 92037), Hanks' solution (standard composition with one modification: the calcium content was replaced by barium or zinc for future analysis by electron probe microanalysis, SEM–EPMA. TBA and toluene were chosen as examples of aggressive solvents; HAc 3%(vol/vol) is often used in biocompatibility assays (see, for example, [4]) and the detergent solutions were used as examples of surfactants. H_2O and Hanks' solution were used as approximations for the physiological environment. Samples were placed in glass test tubes with Teflon screwcaps and immersed in a constant temperature water bath at 37 ± 3 °C for several weeks but not until equilibrium.

The change in thickness was monitored continuously by a thickness gauge with a resolution of 0.2 μm. All swelling tests were performed under the same boundary conditions (sample thickness, exposed area, temperature) where comparisons had to be made.

2.3. DMTA

Dynamic mechanical thermal analysis (DMTA) was performed using a Dupont 983 DMA. A substantial number of control samples were investigated in resonant and fixed frequency modes at 0.5 and 1 Hz. All samples were rectangular, 2 mm thick, approximately 12 mm wide and the clamping distance was 14 mm.

In order to check the consistency of the data, two DMTA machines were compared: the above-mentioned 983 DMA by Dupont Instruments and a DMTA (Model I) by Polymer Laboratories. Under the same experimental conditions, E', E'' and $\tan\delta$ of 10 samples were determined as a function of temperature in the range − 80 to + 60 °C at a 3 °C min^{-1} heating rate.

For the actual DMTA measurements, the same properties were determined both in fixed frequency and resonant frequency modes. As controls, virgin samples of 2-80, 2-87, 3-82, PP and EPDM were taken. To determine the influence of the liquids used, three sets of samples of PP, 2-80, 2-87, 3-82 were soaked in HAc, toluene and the modified Hanks' solution. After fatigue testing, the same measurements were performed on samples of 2-80, 3-82, and 2-87.

2.4. X-ray diffraction

Wide-angle diffraction patterns were recorded by a conventional X-ray diffractometer equipped with a copper tube and nickel filter to examine changes in crystallinity after fatigue tests. In a later stage, additional diffraction patterns were recorded by a Rigaku Rotaflex RU-200B rotating anode (12 kW) equipped with a horizontal Bragg–Brantano focusing diffractometer and a scintillation counter. CuK_α radiation was obtained with a nickel filter. Control samples were 2-80, 2-87 and PP (annealed for high crystallinity and quenched from the melt for low crystallinity).

2.5. SEM

Surface damage and elemental analysis was qualitatively examined by scanning electron microprobe (Jeol 733 Super Microprobe).

2.6. FTIR

Relaxation after fatigue testing was followed by recording FTIR–ATR spectra of the fatigued samples for approximately 500 min after stopping fatigue (Philips PU9800 spectrometer equipped with KRS-5 crystals in a Specac ATR-unit).

3. Results and discussion

3.1. Fatigue

During fatigue on the force-controlled machine, force and displacement are measured in real time. A set of hysteresis curves is collected in Fig. 2. Owing to creep of the sample, the stamp is gradually moved down in order to maintain the initially set boundary-load conditions. The displacement is plotted as a function of the number of fatigue cycles in Fig. 3. From this displacement, the creep was estimated at 2.6% (creep is defined here as the ratio of decrease in sample thickness to initial thickness). The area of the hysteresis curve is proportional to the irreversibly absorbed energy, which gradually decreases from about 4400 J/cycle kg to about 3600 J/cycle kg after 3×10^6 cycles when performed on samples of thickness 2 mm as is clear from Fig. 2. The question now arises whether the combined shear and compression fatigue caused permanent damage to the material. To assess the permanent damage, the response before and after fatigue to solvents or solutions was studied and the modification of the mechanical properties (by DMTA); damage and relaxation were studied kinetically by FTIR (change in crystallinity) and to some extent by XRD.

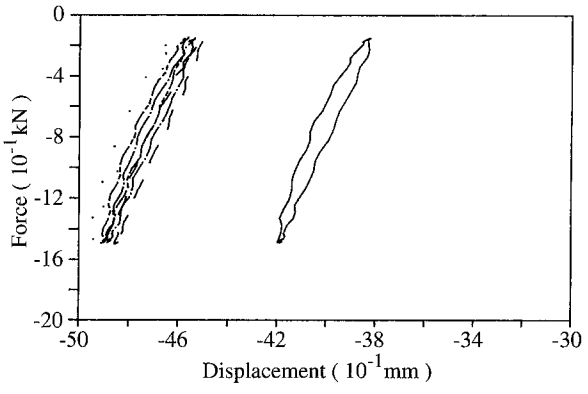

Figure 2 Examples of force–displacement curves (Sample 2.12). Cycle: (—) 3, (– – –) 560 000, (—·—) 1110 001, (—··—) 1670 001, (...) 3330 000

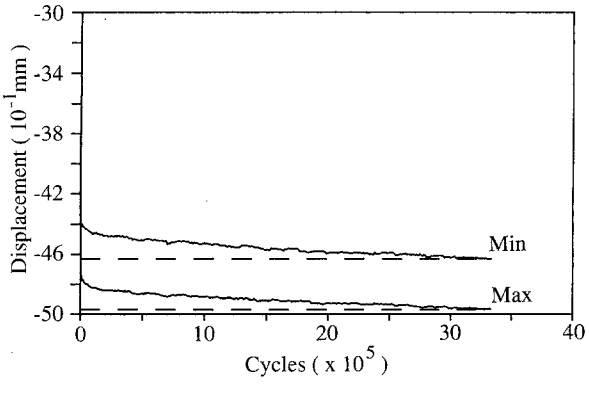

Figure 3 Displacement versus number of fatigue cycles for Sample 2.12.

3.2. Swelling and SEM–EPMA

Preliminary swelling tests were performed to find an appropriate liquid for the actual swelling test resulting in sizeable weight changes of the sample (a few per cent) within reasonable periods of time (a few weeks). The swelling tests were applied (1) as another potentially valuable tool for the assessment of fatigue damage, and (2) to predict long-term absorption behaviour. If cracks are initiated by fatigue, the rate of liquid absorption should increase with respect to virgin samples.

TBA appeared unsuitable because it dissolves some components of the TPO (% δ_m decreases in an irregular way instead of increasing). Most probably, TBA attacks the EPDM or the mineral oil component because there is no known solvent for PP below 80 °C. Toluene shows a relatively high absorption, but the random variations around the expected % δ_m versus time curve are quite large. On the contrary, in water and in the water–Zwittergent solutions, the absorption is very low (2.5% δ_m after 5 weeks at 37 °C). The swelling behaviour of the TPO in Hanks' solution is comparable to the behaviour in H_2O. In HAc, an intermediate swelling occurs and the results are highly reproducible.

Concerning the second point, swelling tests were then repeated with 20 samples of 20 mm × 5 mm for HAc and 4 samples of 20 mm × 20 mm for Hanks' solution. To obtain a graph with dimensionless axes, time was scaled by dividing time values by the time at which % $\delta_m = 0.32$. A graph of % δ_m versus $(\text{time}/\text{time}_{0.32})^{1/2}$ should give a straight line if the absorption is diffusion controlled; after discarding the initial points, a good linear relationship is obtained (regression coefficient $R^2 = 0.991$ and an X-coefficient = 0.76; see Fig. 4). In our opinion, the initial points represent an induction period caused by effects such as surface wetting that interfere with the theoretical behaviour. For the biological screening, samples of 3-82 were immersed in a sterile pyrogen-free solution of NaCl 0.9% (wt/wt) in H_2O in an attempt to extract soluble compounds, but none were found by gas chromatography/mass spectroscopy. Very long-term immersion tests in HAc 3% (vol/vol) are currently being performed and the results will be reported together with those of the *in vivo* and *in vitro* tests. Increase of mass and thickness scales to good approximation as % $\delta_m \sim$ % $\delta_v \sim 3$% δ_l when % δ_l is small. % δ_v, when plotted against $(\text{time}/\text{time}_{0.32})^{1/2}$, gives a reasonably straight line ($R^2 = 0.992$), again after discarding the initial points (Fig. 5). With an X-coefficient of 0.74 there is good correlation between

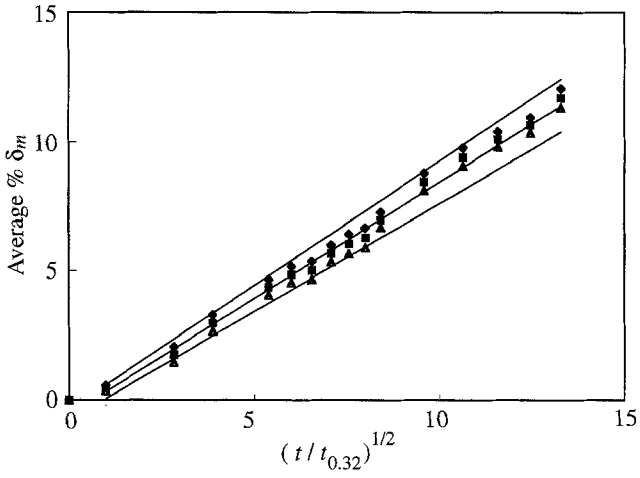

Figure 4 Mass swelling in HAc 3% (vol/vol) of 3-82: average values for % δ_m versus $(t/t_{0.32})^{1/2}$. (■) % δ_m, (◆) % $\delta_m + s$, (▲) % $\delta_m - s$.

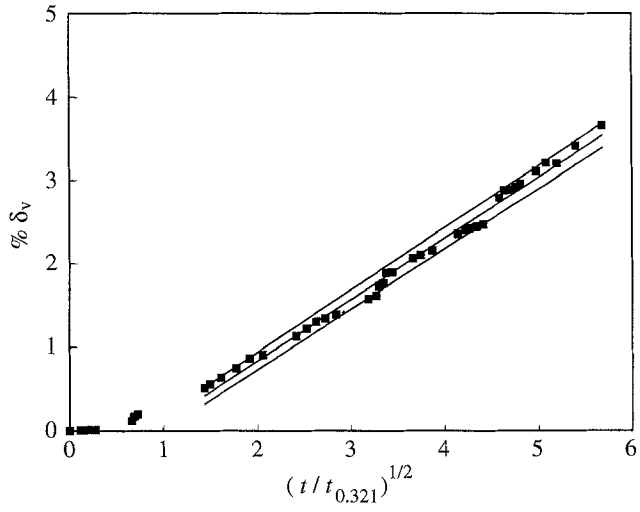

Figure 5 Volume swelling of 3-82 in 3% (vol/vol) HAc: δ_v versus $(t/t_{0.32})^{1/2}$.

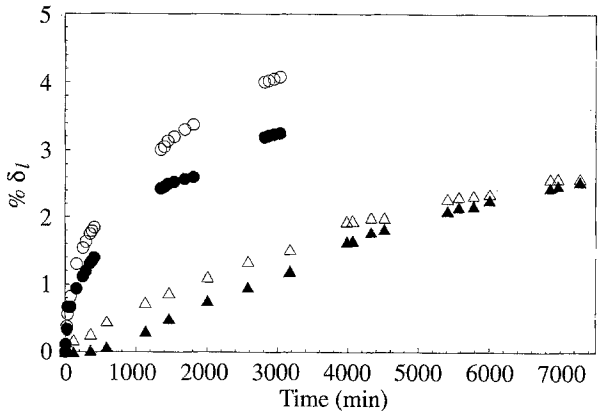

Figure 6 Comparison of volume swelling in 3% (vol/vol) HAc at 65 °C for fatigued (○) 2.2, (●) 2.3, and (△, ▲) virgin 3-82.

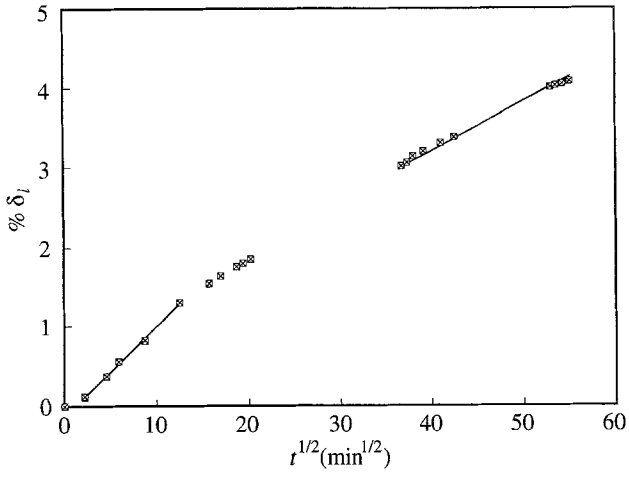

Figure 7 Example of swelling curve % δ_l versus $t^{1/2}$ for a fatigued sample (2.2).

mass-swelling and volume swelling; because the density (at 25 °C) of the TPO (980 kg m^{-3}) is somewhat lower than that of the 3% (vol/vol) HAc (1000 kg m^{-3}), volume swelling should be somewhat less than mass swelling.

After fatigue, swelling tests were conducted in 3% (vol/vol) acetic acid. The average value for δ_m of fatigued samples is 5.04% ($s = 0.5$), for virgin samples 3.9% with a similar standard deviation, when compared after 3 weeks' immersion time at 37 °C. The difference is statistically highly significant ($p < 0.01$). As can be seen in Fig. 6, the swelling rate is quite different for fatigued and virgin samples of 3-82. The data in this figure were collected by accelerated swelling tests (% δ_v) at 65 °C. This is clearly demonstrated by Fig. 7 where the data for one of the fatigued samples is plotted against $t^{1/2}$. Three different parts can be distinguished: a last part which is apparently linear, a first part which is probably linear and a cross-over zone. The last linear part is attributed to diffusion by a similar mechanism as in the virgin samples whereas the first part is assumed to be due to accelerated penetration in microcracks. As these tests were originally intended for damage assessment, no attempts were made to determine diffusion coefficients; only the swelling rate was considered. However, to allow a better interpretation of these results, swelling experiments are currently performed until equilibrium and under the same conditions, i.e. in HAc 3% (vol/vol) and at 65 °C to avoid the difficulties arising from different activation energies at different temperatures of the components of the TPO. Results will be reported in a paper devoted to swelling of this TPO.

The initiation of cracks is one possible explanation for the swelling kinetics. We tried to prove the existence of microcracks by SEM–EPMA. However, the detection of cracks is not easy in elastomers. For this purpose, samples were fractured at liquid nitrogen temperature and the fracture surface inspected by SEM. Existing cracks or crack initiation result in a typical surface topology; this was observed only once in fifteen samples as shown in Fig. 8. Commonly an image as shown in Fig. 9 for a fresh sample is observed.

Another way to observe cracks was the detection of diffusing ions. For this purpose the samples were immersed in Hanks' solution containing Ba^{2+} or Zn^{2+} and barium and zinc images were made with the SEM–EPMA. The elements zinc, iodine, barium or chlorine were present hardly above background levels. A vague pattern of clustered points seems to exist but

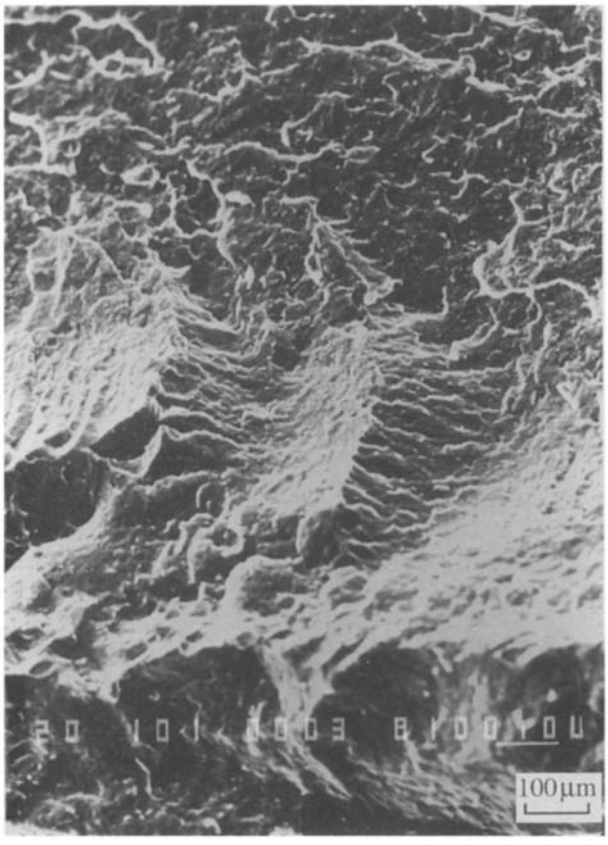

Figure 8 Fracture surface of fatigued Sample 1.4; crack initiation visible. Original magnification ×100.

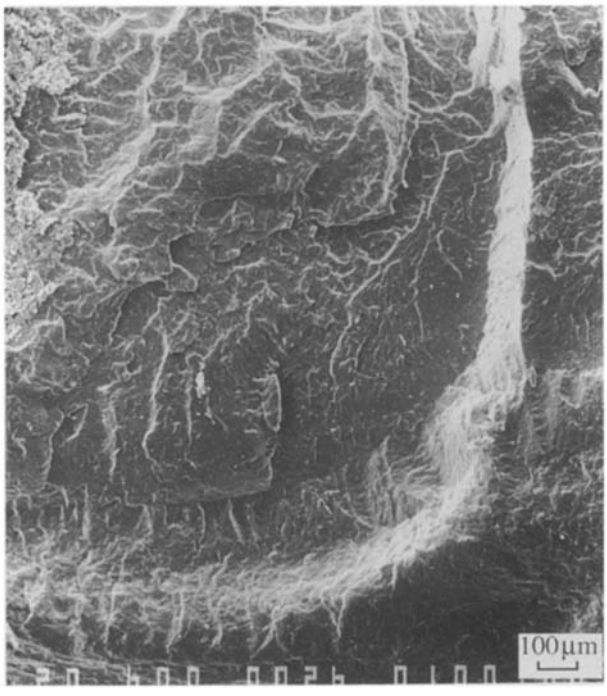

Figure 9 Fracture surface of virgin sample 2-80. Original magnification ×60.

neither proves nor disproves the existence of diffusion paths other than the paths along the presumed random pore structure of the polymer.

The fatigue testing was also expected to have caused surface damage. Therefore, samples were observed by SEM to assess the condition of the surface after fatigue. There appeared to be no significant difference with control samples; surface irregularities are mainly due to the injection-moulding process by which the TPO plates were produced, as can be seen when comparing Figs 10 and 11.

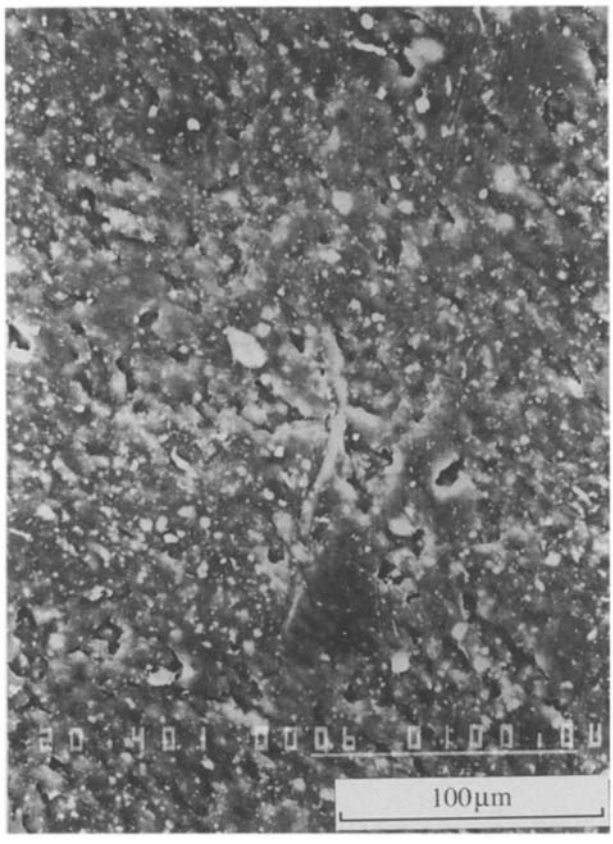

Figure 10 Surface of virgin 3-82; original magnification ×400.

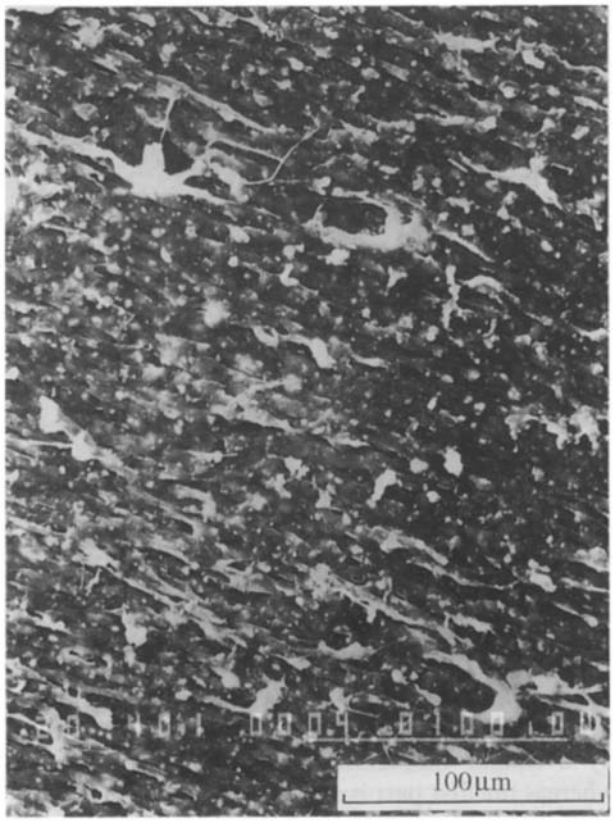

Figure 11 Surface of fatigued 3-82; original magnification ×400.

The stretched lips on the fatigued samples are caused by the friction of the unglued part of the sample against the anvil in the fatigue device (see Fig. 1). The roughness of the anvil drags portions of the softer TPO sample along during insertion of the sample at the start of the fatigue. The deformation of the TPO is partly irreversible which results in the typical morphology of lips. Engel *et al.* [6] described this surface damaging mechanism in greater detail. This deformation must have happened during the initial period of the experiment because the degree of lip formation does not seem to increase with increasing number of fatigue cycles (based upon visual inspection of the micrographs). Some increase in surface roughness should not be excluded but it is not sufficient to explain the increase in solvent absorption, because increased roughness cannot alter the bulk diffusion process. Only the initial induction period might be influenced by it and should then be shorter for fatigued samples, but this phenomenon has not been exploited further.

3.3. DMTA

3.3.1. Comparison of 983 Dupont and DMTA PL

As will be clear later on, the subtle variations observed by this and other techniques require a careful examination of possible instrumental artefacts. For this purpose, two DMTA instruments were compared. Ten samples 2-80 were tested in fixed frequency mode at 0.1, 0.3, 5, 10 and 20 Hz; all measurements were repeated on a different sample to investigate reproducibility. Results for 10 and 20 Hz had to be discarded because the 983 DMA appeared unsuitable for measurements at these frequencies in the fixed frequency mode (although the instruments' specifications state a 0.001–10 Hz range for fixed frequency measurements).

As a general conclusion of the intercomparison of these instruments, it can be said that the shapes of the E', E'' and tan δ curves are identical, but that there is a slight temperature shift of the transitions. The glass transition temperature, T_g, was determined either as the maximum of the E'' curve or as the maximum of the tan δ curve. Results are shown in Table III for E''. Conventionally, however, the peak of tan δ is used for determining T_g; these results are shown in Table IV. Note that there are two clear tan δ peaks in the T-domain and only one E'' peak; this is because tan δ, defined as E''/E', is a more sensitive indicator for T_g than E''.

From these data it is clear that the PL instrument measures the transitions at slightly lower T-values than the Dupont instrument; temperature differences are approximately as follows: 2 °C on E''; 3 °C on the tan δ at low T (approximately − 40 °C) at 0.1 and 0.3 Hz and 5 °C at 5 Hz; 8 °C on the tan δ at high T (approximately + 10 °C) at 0.1 and 0.3 Hz and 5 °C at 5 Hz.

A general interpretation of DMTA graphs in terms of T_g, secondary transitions, width of the E'' peaks as a measure of crystallinity, etc., can be found elsewhere

TABLE III Comparison of E'' peaks in the temperature domain

Frequency (Hz)	E'' peak position in T domain (°C)			
	983 DMA Dupont		DMTA Polymer Labs	
	1st sample	2nd sample	1st sample	2nd sample
0.1	− 43	− 43	− 45	− 45
0.3	− 42	− 42	− 44	− 44
5	− 38	− 38	− 40.5	− 41.5
9	− 40	n.m.[a]	n.a.[b]	n.a.
10	n.m.	n.m.	− 40.5	− 40.5
20	n.m.	n.m.	− 38.5	− 39

[a] n.m.: not measurable on this instrument.
[b] n.a.: not measured.

TABLE IV Comparison of tan δ peaks in temperature domain

Frequency (Hz)	Tan δ peak position in T domain (°C)			
	983 DMA Dupont		DMTA Polymer Labs	
	1st sample	2nd sample	1st sample	2nd sample
0.1	− 40	− 38	− 43	− 42
	− 0.5	2	− 6.5	− 6
0.3	− 39	− 36	− 41	− 41
	4	7	− 4	− 4
5	− 38	− 38	− 39	− 37.5
			10	10
9	− 32.8	n.m.	n.a.	n.a.
	Noise[a]			
10	n.m.	n.m.	− 38	− 36
			8	9
20	n.m.	n.m.	− 36.5	− 34.5
			10.5	12.5

[a] Noise: too much noise to determine tan δ peak maximum accurately.

[7]. For the TPO, the two peaks in E'' and tan δ are attributed to the T_g transition of EPDM (at approximately − 40 °C) and PP (at approximately 10 °C) (see Fig. 12). This was confirmed by DMTA measurements of pure PP and EPDM (cured in the laboratory for 2 h at 180 °C) and peaks in tan δ and E'' at the previously mentioned positions were found. Note that the T_g of PP is substantially higher than listed in textbooks (e.g. [8]) but this difference has to be attributed to the different experimental procedure for determining T_g (DSC versus DMTA).

On the DMTA graphs of soaked samples, a broadening of the tan δ and E'' peaks was observed which might be due to absorbed liquid, but usually points to an increase of the crystallinity [7]. Interpretation of DMTA measurements in terms of crystallinity will be discussed further in the text, together with the interpretation of the FTIR and XRD results.

Further control of the congruency of our DMTA data is supplied by application of the time–temperature superpositioning principle where the shift factors are calculated according to the WLF model. Frequency multiplexing runs at 0.1, 0.32, 1, 3.2 and 8 Hz were performed on fresh and fatigued samples of 3-82 in the temperature range − 70 to − 10 °C. Using the time–temperature superposition

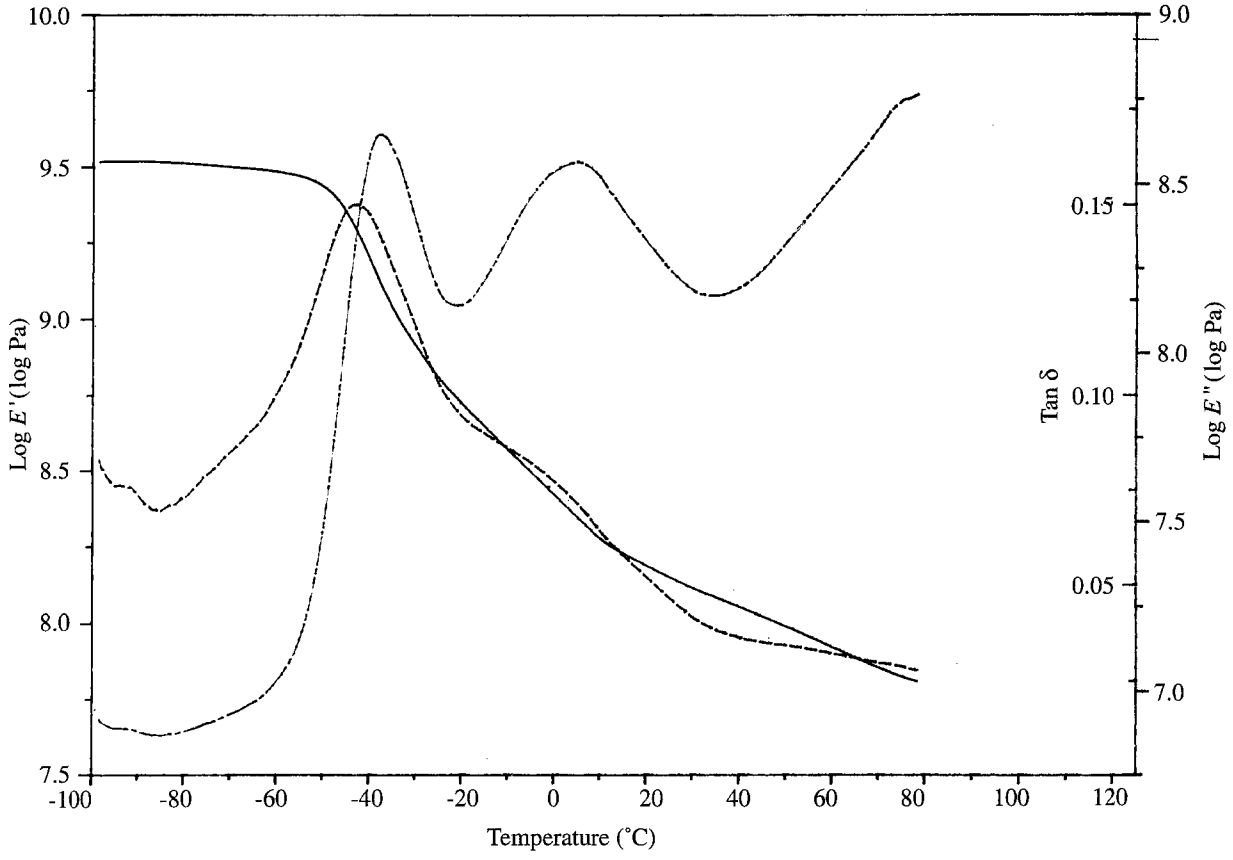

Figure 12 DMTA plot for 2-80: (—) E', (- - -)E'' and (— · —) tan δ versus temperature. Amplitude ($p - p$) = 0.30 mm.

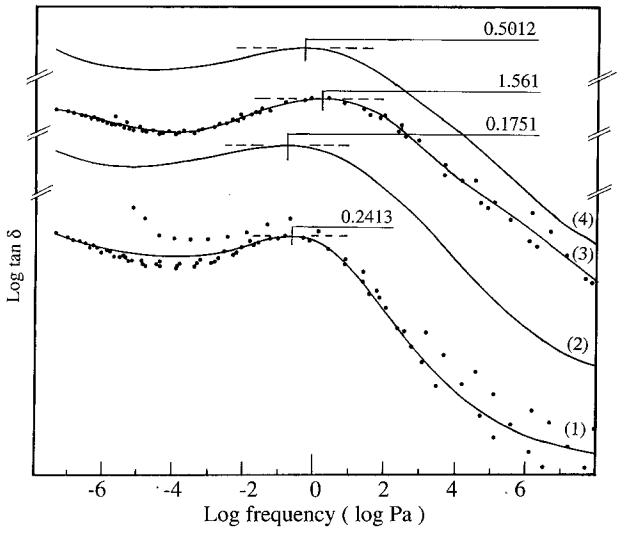

Figure 13 Examples of master curves for log(tanδ) versus log(frequency). (1) control; (2) 4×10^5 cycles; (3) 2×10^6 cycles; (4) 5×10^6 cycles; for clarity, data points omitted on curves 2 and 4. Log(tanδ) ≈ −0.6 (max).

principle, the obtained data were shifted horizontally in the frequency domain to obtain a log(tan δ) –log(frequency) master curve for the transition at −40 °C. The time–temperature superposition principle states that with polymers, data on long-term behaviour at lower temperatures can be obtained by performing short-term experiments at elevated temperatures [9]. This can be understood if one considers that the viscoelastic properties of polymers are determined by the mobility of the macromolecules in the polymer and this mobility is enhanced on increasing temperature [7]. The log(tan δ)–log(frequency) master curve for the T_g transition of EPDM shows a flat maximum at ≈ 0.24 Hz for the control samples. For fatigued samples, the high-frequency part of the master curve shifts horizontally mostly to higher frequencies but with data scattered between 0.17 and 1.95 Hz (see Fig. 13). This means that maximal damping occurs at slightly higher frequencies, i.e. the stiffness increases. For better understanding of the changes in the material by fatigue, a detailed investigation by small-angle neutron scattering (SANS) is set up. One would expect a relationship between the frequency at maximum and the number of fatigue cycles. However, a clear relation cannot be found because of the scatter of the results (due to the flat maximum), although a Kendall S-test gives a significance level of 2.5% when applied to the data.

3.4. X-ray diffraction (XRD)

On a wide-angle diffraction pattern of any grade of the TPO investigated, all peaks can be attributed to crystal plane reflections of PP [10] only (Fig. 14).

Care must be taken when diffraction patterns are recorded in reflection geometry. In this case, the $hk1$ reflections are weakened due to orientational or sample boundary effects. On patterns collected in transmission geometry, all PP reflections are present.

Crystallinity indices were calculated relative to a highest crystalline and a lowest crystalline standard as described by Vonck and Balta-Calleja [11] and Alexander [12]. Results have not yet been reported be-

cause it was difficult to obtain consistent results (due to insufficient difference in crystallinity between the standards).

Line narrowing occurs after fatigue, indicating an increase of the crystallite size according to the Scherrer formula (Fig. 15).

$$t = 0.9\lambda/(B\cos\theta_B) \quad (3)$$

where λ is the wavelength of the radiation, t the crystallite size, θ_B the Bragg angle and B the FWHM of the reflection at $2\theta_B$. From the FWHM of the 1 1 0 reflection at 14° 2θ, a crystallite size of 8.6 nm was calculated for virgin 3-82, whereas the fatigued samples 2.9 and 2.10 had crystallite sizes of 8.8 and 9.7 nm, respectively. When recording the XRD patterns, care was taken to ensure equal experimental conditions for all measurements.

As will be discussed below, FTIR data point to a small increase in crystallinity by fatigue and after removal of the load, crystallinity relaxes to values near those of the fresh sample. The IR observations led us to expect a change in crystallinity from the XRD and a consistent increase in E'' peak width from DMTA. However, this increase was only verified for the XRD and not for the E''. Why?

The only compound partly crystalline in the elastomer is PP. To the best of our knowledge, no data relating E'' and crystallinity for PP exist. So, we must

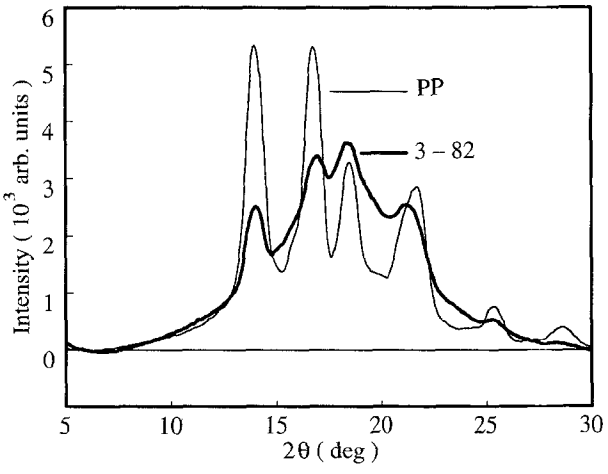

Figure 14 Wide-angle XRD patterns for PP and 3-82, recorded in transmission geometry (X-ray source: rotating anode).

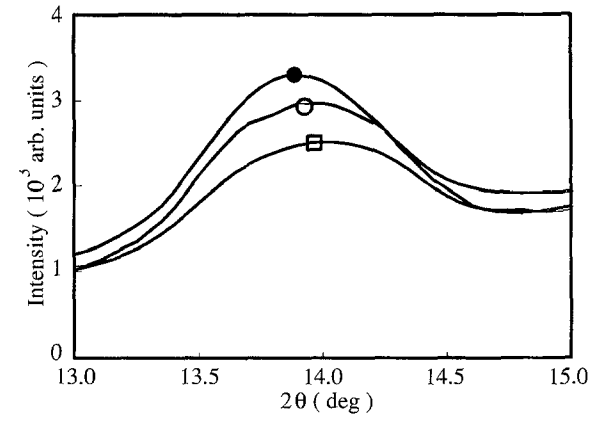

Figure 15 Wide-angle pattern of (□) virgin 3-82 and fatigued samples (○) 2.9 and (●) 2.10.

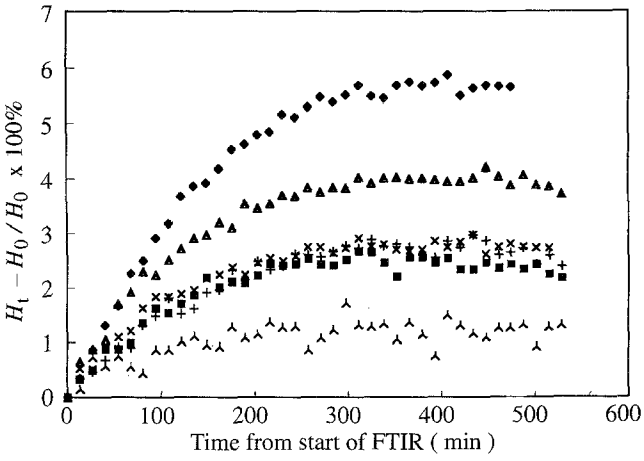

Figure 16 Relaxation kinetics of control and fatigued samples (■) 2.1, (◆) 2.2, (▲) 2.4, (×) 2.7, (+) 2.5 and (λ) control by FTIR. In the ordinate, the relative increase in the ratio A_{1168}/A_{974} is plotted versus relaxation time.

rely on assumptions based on data obtained on other polymers. XRD data for polyetheneterephtalate (PET) show that there are two levels for the E'' peak widths: one corresponding to a crystallinity ranging from 0–12% and another for crystallinity > 18% with a transition zone in between [7]. This means that, except for the threshold domain, E'' is fairly independent of crystallinity. X-ray crystallinity does not change much (if at all) and E'' only slightly. Consequently, if we accept similar relationships to exist for PET and PP, the structural changes induced by fatigue are assumed negligibly small, but it should be stressed that the sensitivity of the XRD data to changes in E'', and *vice versa*, is rather low if the relationships are similar to the PET case.

3.5. FTIR

The damage by fatigue is apparently small as is demonstrated by all the results discussed thus far. The XRD as well as the FTIR experiments were set up in such a way that relaxation, if happening at all, could be detected. XRD refers to the intraparticle ordering and the size of cyrstallites, FTIR refers mainly to intramolecular and partly intermolecular changes. The absorbance bands at 1168 and 974 cm^{-1} are pseudocrystalline peaks. The ratio A_{1168}/A_{974} is proportional to the helicoidally ordered portion of PP [13]. Relaxation (by change of this ratio after stopping the fatigue experiment) is detectable but hardly different from the small relaxation always present when an elastomer sample is compressed between the ATR-crystal and the metal backing plate. In all cases the apparent degree of crystallinity is superior to the control (Fig. 16).

4. Conclusion

A detailed study of the fatigue behaviour of a laboratory-made medical grade TPO, similar to commercially available TPOs, is presented. The components of the TPO were all FDA-regulated compounds, and processing was performed in specially purged equipment with no residue from previous batches. The

investigation was undertaken after a biological screening for compliance with USP Class VI requirements, which did not exclude potential endoprosthetical use of the TPO. Uptake of water and/or ions is not high as derived from swelling tests (below 5% mass increase after 5 weeks at 37 °C). The material was subjected to the combined action of cyclic shear and compression loading.

Definite but very slight modification of the material is observed. Creep under the experimental conditions described remains below < 3% (from displacement of the hysteresis curve during fatigue; Fig. 3). Because the fatigue tests only involved the 3-82 and the 2-80 grades of the TPO, the difference in hardness was too small (82 Shore A compared with 80 Shore A) to study the influence of this parameter on creep. The dissipated energy during a fatigue cycle gradually decreases as a function of the number of cycles from 4400 J/cycle kg to 3600 J/cycle kg (Fig. 2). After fatigue, the swelling rate in HAc solutions is definitely increased (Fig. 6). In order to explain these modifications, macromechanical damage, i.e. initiation of cracks, and/or inter- and intramolecular modifications have been assumed.

4.1. Cracks

The increased swelling rate in HAc solution was assumed to be due to cracks, being penetration paths for liquids far more accessible than pores from the natural porosity of the polymer. For testing this hypothesis, the samples were put into contact with Hanks' solution in which calcium was replaced by barium or zinc (because calcium is a very common contaminant). Barium and zinc images of sections parallel to and perpendicular to the sample surface were produced by SEM–EPMA. Signals, hardly above background, allowed us to presume such diffusion paths, but were not sufficient to prove their existence. SEM images of surfaces after fracturing at liquid nitrogen temperature, however, point in the direction of cracks. External surface damage, e.g. roughening, would be another possibility, but microscopic comparisons of surfaces before and after fatigue do not seem to favour this explanation.

4.2. Inter- or intramolecular modification

FTIR spectra do not elucidate any intramolecular changes. Kinetic measurements, however, revealed a slight relaxation to a higher degree of crystallinity (intermolecular ordering) after removing the load. The same kinetics were not found by XRD, but careful analysis of the diffractograms points to an increase of the size of crystalline domains. These observations are in agreement with the shifts in $\tan\delta$ derived from dynamic mechanical measurements.

All the experimentally observed changes induced by fatigue were very small. For this reason, great attention was paid to instrumental artefacts and data handling (comparison of DMTA instruments, analysis of FTIR and XRD data). Consequently, we concluded that the TPOs involved in the fatigue experiments (2-80 and 3-82) exhibit a fairly satisfactory resistance to fatigue and that the observed modifications are very similar for the standard-grade 2-80 and the medical-grade 3-82. More specifically, the applied cyclic stresses are probably below the endurance limit, σ_e, of the TPOs for the applied deformation mode. The ultimate choice of which hardness to use depends on the type of prosthesis used and must be determined by testing (both *in vivo* and *in vitro*) on prosthesis models. The biological screening and the swelling behaviour, together with the mechanical properties, allow further medical *in vitro* and *in vivo* studies to proceed. These studies are underway and the intermediate results are promising. The results of these experiments will be reported later.

Acknowledgements

A grant of IWONL to S. Jaecques (910219) is gratefully acknowledged. The authors thank Ing. J. Mariën for his excellent technical assistance with the fatigue experiments.

References

1. M. S. REISCH, *Chem. Eng. News*, 4 May (1992) 29.
2. United States Pharmacopeia, Vol. XX (US Pharmacopeial Convention, Rockville, MD, 1980) pp. 950–1.
3. C. P. RADER and S. ABDOU-SABET, in "Thermoplastic elastomers from rubber-plastic blends" (Ellis Horwood, Chichester, England, 1990) p. 159–97.
4. "Annual Book of ASTM Standards, Section 13: Medical Devices, F813", Vol. XV (ASTM, Philadelphia, PA, 1984, reapproved without revision 1986) pp. 329–32.
5. F. MAST and H. A. HUYSMANS, in "IVth World Biomaterials Congress", Berlin 24–28 April 1992, abstracts, p. 692.
6. L. ENGEL, H. KLINGELE, G. W. EHRENSCHEIN and H. SCHAPER, "An Atlas of Polymer Damage" (Wolfe Science, Carl Hanser, München, Vienna, 1981).
7. T. MURAYAMA, "Dynamic Mechanical Analysis of Polymeric Material" (Elsevier, Amsterdam, 1978).
8. R. C. Weast (ed.), "CRC Handbook of Chemistry and Physics", (Chemical Rubber Co., OH, 1991).
9. U. EISELE, "Introduction to Polymer Physics" (Springer, Berlin Heidelberg, 1990) pp. 40–3.
10. J. W. TURLEY, "X-Ray Diffraction Patterns of Polymers" (Dow Chemical Co., Midland, MI, USA, 1965).
11. C. G. VONCK and F. J. BALTA-CALLEJA, "X-Ray scattering of synthetic polymers" (Elsevier, Amsterdam, 1989).
12. L. E. ALEXANDER, "X-Ray Diffraction Methods in Polymer Science" (Krieger, Huntington, NY, 1979) pp. 176–88.
13. M. FUYIYAMA, H. AWAYA and K. AZUMA, *J. Polym. Sci. Polym. Lett. Ed.* **18** (1980) 105.

Received 18 August 1992
and accepted 2 February 1993